Accelerated and noise-resistant generation of high-fidelity steady-state entanglement with Rydberg atoms

Ye-Hong Chen,[1,2] Zhi-Cheng Shi,[1,2] Jie Song,[3] Yan Xia,[1,2,*] and Shi-Biao Zheng[1,2]
[1]*Department of Physics, Fuzhou University, Fuzhou 350116, China*
[2]*Fujian Key Laboratory of Quantum Information and Quantum Optics, Fuzhou University, Fuzhou 350116, China*
[3]*Department of Physics, Harbin Institute of Technology, Harbin 150001, China*

(Received 12 October 2017; revised manuscript received 11 February 2018; published 20 March 2018)

Based on Lyapunov control, a scheme is proposed to accelerate dissipation dynamics for the generation of high-fidelity entanglement between two Rydberg atoms in the context of cavity QED. We first use quantum Zeno dynamics and the Rydberg antiblockade to find a unique steady state (two-atom singlet state) for the system. Then, we apply additional coherent control (ACC) fields to improve the evolution speed of the dissipative system. The ACC fields are designed based on the target state and they vanish gradually along with increasing of the fidelity; thus, the system is guaranteed to be finally stable. Additionally, the current accelerated scheme is checked to be robust against systematic and amplitude-noise errors.

DOI: 10.1103/PhysRevA.97.032328

I. INTRODUCTION

There is now growing interest in obtaining accelerated dynamics because fast and noise-resistant schemes are natural requirements in quantum information processing. The accelerated dynamics is also expected to have the ability to restrain the accumulated negative effect caused by dissipation during a long time evolution. For instance, an approach named "Shortcuts to adiabaticity" (STA) [1] combining the advantages of (fast) resonant pulses and (robust) adiabatic techniques has attracted much attention in recent years [2–16] and been applied in fields including fast population transfer [17–19], fast entanglement generation [20–22], fast quantum computation [23], and so on [24–28]. However, "shortening the time always implies an energy cost" [6,9,14,29,30], and one can usually find the intermediate states are populated into a relatively high level by using STA for the goal of accelerating [4–6]. In recent schemes for fast entanglement generation based on STA in atomic systems [20–22], since the intermediate states are excited, the negative effect caused by dissipation does not decrease remarkably even though the evolution time is significantly shortened. There exists a tradeoff between the total evolution time and the populations of excited states [29,30]. That is, directly shortening the evolution time seems unable to restrain the negative effect caused by dissipation in atomic systems for quantum entanglement generation.

On the other hand, rather than considering dissipation as a detrimental effect, recent studies have changed the view for dissipation due to the fact that the environment can be used as a resource for quantum computation and entanglement generation [31–37]. Currently, there are several representative schemes creating steady entanglement of high quality by dissipation [38–56]. For instance, two groups independently proposed theoretical schemes to prepare high-fidelity steady-state entanglement between a pair of Rydberg atoms with dissipative Rydberg pumping [49,50]. In 2011, Krauter *et al.* experimentally realized a steady-state entanglement of two macroscopic objects by dissipation [46]. In general, by using dissipation dynamics to generate atomic entanglement in cavity QED systems, the fidelity F of the target state is in a relationship $(1-F)\propto C^{-1}$ with the cooperativity $C=g^2/(\gamma\kappa)$ [31], where g is the atom-cavity coupling strength, γ is the atomic decay rate, and κ is the cavity decay rate. A large cooperativity is always necessary in order to obtain a high-fidelity entanglement. However, a large cooperativity leads to a very long convergence time (total evolution time) that is also unwelcome [31,45,57]. It would be a serious issue to realize large-scale integrated computation if taking too long for entanglement generation. We are thus guided to ask, is it possible to accelerate the slow dissipation dynamics without losing its advantages?

The idea of combining advantages of resonant pulses and adiabatic techniques in STA inspires us that combining advantages of dissipation dynamics and another (fast) dynamics may be a good idea to solve the problem. Therefore, in this paper, we combine dissipation dynamics with coherent unitary dynamics and propose a promising scheme for an accelerated and dissipation-based entanglement generation. We add target-state-related additional coherent control (ACC) fields into the dissipation process. The intensities of the ACC fields are designed to decrease with the increasing of fidelity for the target state. To realize such an idea, we use Lyapunov control which may have the ability to shorten the convergence time of an open system as pointed out by Yi *et al.* in Ref. [63]. Lyapunov control is a form of local optimal control with numerous variants [58–63] and has been used to manipulate open quantum systems [63–66]. In this case, the evolution of the system can be understood as two stages.

(i) The first stage is mainly governed by the ACC fields. The evolution in this stage is nearly unitary so that the system can

*xia-208@163.com

be rapidly driven to the target state with fidelity about 90%. In this stage, the target state is not a steady state of the system.

(ii) The second stage is mainly governed by the dissipation dynamics. When the fidelity for the target state is ∼90%, the intensities of the ACC fields become very small and their effects on the dynamics can be ignored. The dissipation dynamics thus governs the system to converge to the target state with fidelity increasing from ∼90 to ∼100%. In this stage, the target state is the unique steady state of the system.

Since the evolution is accelerated in the first stage, the total evolution time required in the current scheme is much shorter than that in a general dissipation-based scheme. This idea is verified by an atom-cavity system via quantum Zeno dynamics [67] and the Rydberg antiblockade in this paper. Regarding two typical dissipation sources in a cavity QED system, we make use of atomic decay but avoid the effect of cavity decay based on quantum Zeno dynamics. The Rydberg antiblockade as shown theoretically in Refs. [51–53] can accelerate the convergence rate of stationary entanglement, since the strength of antiblockade interaction is much larger than the Rabi frequency of the microwave field. The ACC fields are chosen as the easily realized classical drivings. Their intensities are designed as functions of the system's evolution speed v (the time derivative of fidelity). For $t \to t_f$ (t_f is the final time), the system gradually becomes stable, i.e., $v|_{t\to t_f} \to 0$, that guarantees the ACC fields vanish gradually along with the increasing of time. Hence, a fidelity ∼95% of steady-state entanglement is available even with evolution time $t_f = 250/g$.

The paper is organized as follows. In Sec. II, we guarantee a unique entangled steady state is existent by using quantum Zeno dynamics and the Rydberg antiblockade. In Sec. III, we define the evolution speed for the system and show how to accelerate the dissipation dynamics. In Sec. IV, we give the analysis and discussion on the accelerated dynamics. In Sec. V, we verify the robustness of the scheme against stochastic parameter fluctuations that generally exist in the driving fields. Conclusions are given in Sec. VI.

II. STEADY GROUND-STATE ENTANGLEMENT OF TWO ATOMS

We consider a system consisting of two N-type four level Rydberg atoms (marked as atom A and atom B), and the relevant configuration of the atomic level is illustrated in Fig. 1(a). We first consider that $\Pi_{A,(B)} = \varpi_{A,(B)} = 0$, and the system is thus the same as that in Ref. [51]. In the regime of the Rydberg antiblockade, $U_{rr} \sim 2\Delta \gg \Xi_{A,(B)}$, and the Hamiltonian [51] for the current system reads

$$\begin{aligned} H_0 =& H_r + H_{ac}, \\ H_{ac} =& \sum_{n=A,B} g_n |p\rangle_n\langle g|a + \text{H.c.}, \\ H_r \approx& \sum_{n=A,B} (\Omega_n |e\rangle_n\langle p| + \omega_n |g\rangle_n\langle e|) + \lambda |ee\rangle\langle rr| + \text{H.c.}, \end{aligned} \tag{1}$$

where U_{rr} is the Rydberg-mediated interaction [68–73] and $\lambda = 2\Xi^2/\Delta$ ($\Xi_A = \Xi_B = \Xi$) is given according to the second-order perturbation theory [74]. The dynamics of the system in this case is modeled by the Lindblad-Markovian master equation [75] as

$$\begin{aligned} \dot{\rho} =& -i[H_0, \rho] + \mathcal{L}\rho, \\ \mathcal{L}\rho =& \sum_k L_k \rho L_k^\dagger - \tfrac{1}{2}(L_k^\dagger L_k \rho + \rho L_k^\dagger L_k), \end{aligned} \tag{2}$$

where the overdot denotes the time derivative and the Lindblad operators are

$$\begin{aligned} L_{n,1} =& \sqrt{\gamma/2}|g\rangle_n\langle p|, \quad L_{n,2} = \sqrt{\gamma/2}|e\rangle_n\langle p|, \\ L_{n,3} =& \sqrt{\Gamma}|e\rangle_n\langle r|, \quad L_4 = \sqrt{\kappa}a \quad (n = A, B). \end{aligned} \tag{3}$$

L_4 denotes the cavity decay with decay rate κ.

Then, similar to Ref. [51], by applying quantum Zeno dynamics (see the Appendix for details) under the strong-coupling limit $\Omega_{A,(B)}, \omega \ll g$, the effective Hamiltonian takes the following concise form [51]:

$$\begin{aligned} H_{\text{eff}} \simeq& \Omega |T\rangle\langle\phi_0| + \sqrt{2}\omega |T\rangle(\langle gg| + \langle ee|) \otimes |0\rangle_c\langle 0| \\ &+ \lambda |ee\rangle\langle rr| \otimes |0\rangle_c\langle 0|, \end{aligned} \tag{4}$$

where $\Omega = \Omega_B = -\Omega_A$, $|\phi_0\rangle = (|pg\rangle - |gp\rangle) \otimes |0\rangle_c/\sqrt{2}$, and $|T\rangle = (|eg\rangle + |ge\rangle) \otimes |0\rangle_c/\sqrt{2}$. For the sake of simplification, we choose $g_A = g_B = g$ and $\omega_A = \omega_B = \omega$ in obtaining the effective Hamiltonian. The corresponding effective Lindblad operators in the Zeno Z_0 subspace are [51]

$$\begin{aligned} L_1^e =& \sqrt{\frac{\gamma}{4}}|S\rangle\langle\phi_0|, \quad L_2^e = \sqrt{\frac{\gamma}{4}}|T\rangle\langle\phi_0|, \\ L_3^e =& \sqrt{\frac{\gamma}{2}}|gg\rangle \otimes |0\rangle_c\langle\phi_0|, \end{aligned} \tag{5}$$

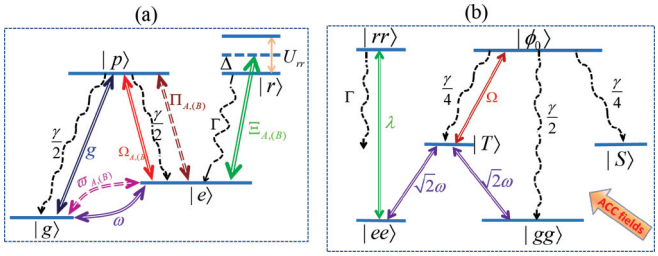

FIG. 1. (a) Schematic view of atomic-level configuration. The atomic transition $|g\rangle_{A,(B)} \leftrightarrow |p\rangle_{A,(B)}$ is coupled to a quantized cavity field with coupling strength g and the transition $|e\rangle_{A,(B)} \leftrightarrow |p\rangle_{A,(B)}$ is driven by two optical pumping lasers with Rabi frequency $\Omega_{A,(B)}$ and $\Pi_{A,(B)}$. In addition, two microwave fields of Rabi frequency $\omega_{A,(B)}$ and $\varpi_{A,(B)}$ are introduced to cause transition between ground states $|g\rangle_{A,(B)}$ and $|e\rangle_{A,(B)}$, and an extra pumping laser field with Rabi frequency $\Xi_{A,(B)}$ drives the atom to the high-lying excited Rydberg state $|r\rangle_{A,(B)}$ from state $|e\rangle_{A,(B)}$ by detuning $-\Delta$. $\Pi_{A,(B)}$ and $\varpi_{A,(B)}$ are the Rabi frequencies for ACC fields given according to the Lyapunov control. (b) The effective transitions for the two-atom system. The whole system works well in the so-called Zeno Z_0 subspace of zero occupation for the cavity mode due to the quantum Zeno dynamics. With the effective driving fields and decays, ultimately, the system will be stabilized into the state $|S\rangle$. The ACC fields mainly accelerate the transitions $|gg\rangle \to |T\rangle \to |\phi_0\rangle \to |S\rangle$ and $|gg\rangle \to |S\rangle$ to shorten the evolution time.

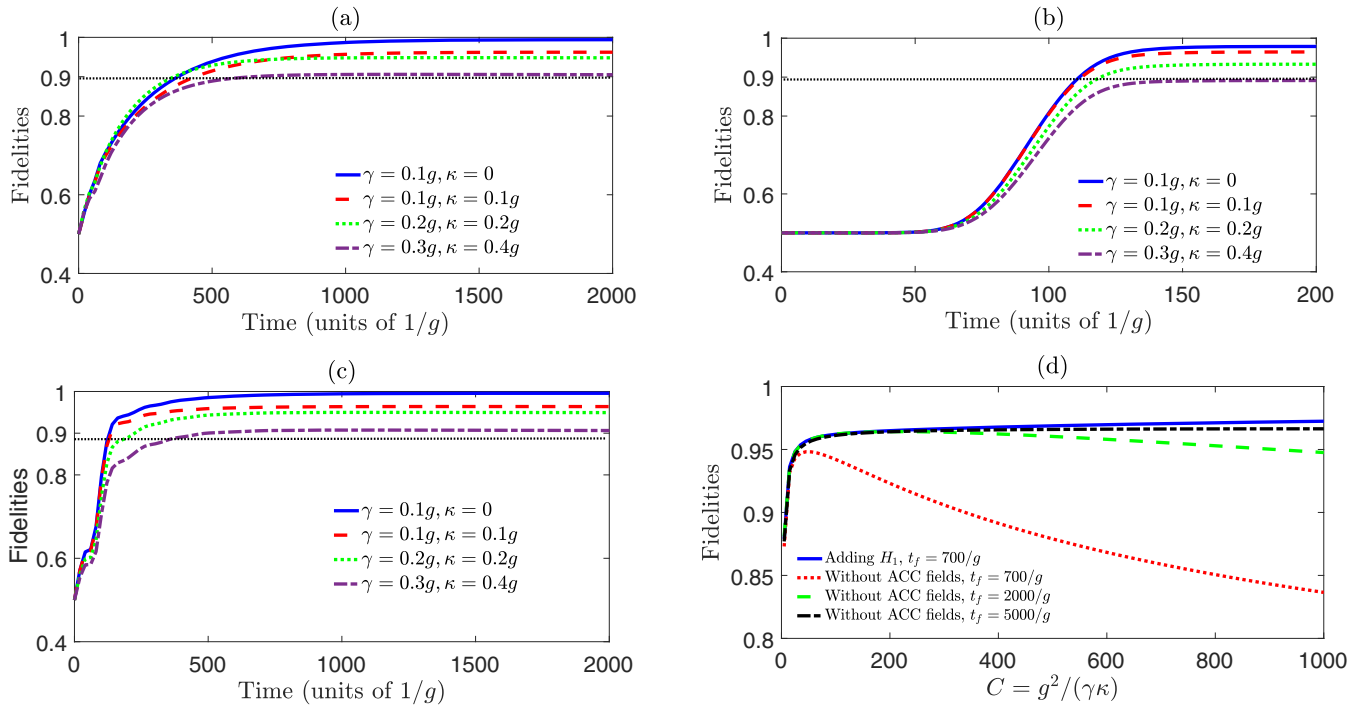

FIG. 2. Time evolutions of different schemes when decays are considered and the initial state is $|eg\rangle \otimes |0\rangle_c$. (a) Based on a dissipation-based scheme with the Hamiltonian in Eq. (1). Parameters are $\Omega = 0.07g$, $\omega = 0.02g$, $\Xi = 5g$, and $\Delta = 100g$. (b) Based on a STIRAP scheme with the Hamiltonian in Eq. (7). Parameters are chosen as $t_o = 20/g$, $t_c = 35/g$, and $\Omega_0^{\rm adi} = 0.15g$. (c) Based on a speed-up scheme by adding ACC fields with $\mu_1 = 0.3g$ into the dissipative system. Parameters are the same as Fig. 2(a). (d) Comparison between dissipation-based schemes with and without ACC fields. The red dotted, green dashed, and black dot-dashed curves represent the fidelities vs C of a traditional dissipation-based scheme with parameters the same as Fig. 2(a). The blue-solid curve represents the fidelity vs C when ACC Hamiltonian H_1 is applied into the system with intensity-dependent coefficient $\mu_1 = 0.3g$. We assume $\gamma = \kappa$ in plotting Fig. 2(d).

where $|S\rangle = (|eg\rangle - |ge\rangle) \otimes |0\rangle_c/\sqrt{2}$, Here the spontaneous emission of the Rydberg state is neglected according to the realistic situation that $\Gamma \ll \gamma$. Clearly from Eqs. (4) and (5), we find a steady state $|S\rangle$ for the effective system on account of $H_{\rm eff}(L_k^e)|S\rangle = 0$ and $(L_k^e)^\dagger|S\rangle \neq 0$ $(k = 1,2,3)$. Thus, for an arbitrary initial state, it will be finally converged into the steady state $|S\rangle$ by the process of pumping and decaying as shown in Fig. 1(b).

III. THE EVOLUTION SPEED AND THE PRINCIPLE OF ACCELERATION

The last section presents a method to generate an entangled steady state $|S\rangle$ by dissipation. However, the generation process is usually unsatisfactorily slow. We define the fidelity for the target state $|S\rangle$ as $F = \langle S|\rho|S\rangle$. The instantaneous speed of the evolution can be thus defined as

$$v = \partial_t F = \langle S|\dot{\rho}|S\rangle = \frac{\gamma}{4}\langle\phi_0|\rho|\phi_0\rangle, \tag{6}$$

which depends on the spontaneous emission rate γ and the instantaneous population for the effective excited state $|\phi_0\rangle$. The spontaneous emission rate and the population for $|\phi_0\rangle$ are, however, both small in the dissipation system when a high fidelity is required [31]. As we know, the fidelity of a dissipation-based scheme is usually proportional to the cooperativity C according to the relationship $1 - F \propto C^{-1}$ [31]. The cooperativity C, however, is inversely proportional to decay rates. Hence, in order to obtain a high-fidelity entanglement generation, small decay rates γ and κ are necessary for a dissipation-based scheme, which lead to a long convergence time [51] [see Fig. 2(a)]. Figure 2(a) shows the fidelity versus time with different decay rates. Obviously from the figure, the time required to stabilize the system into the target state $|S\rangle$ increases with the decreasing of the cooperativity C. For example, for $C = 100$ corresponding to $\gamma = \kappa = 0.1g$, the convergence time is about $t_f = 1100/g$, while for $C = 8.33$ corresponding to $\gamma = 0.3g$ and $\kappa = 0.4g$ the convergence time is about $t_f = 800/g$. However, the evolution is still slow in comparison with a stimulated Raman adiabatic passage (STIRAP) scheme as shown in Fig. 2(b), which is displayed based on an interaction Hamiltonian

$$H^{\rm adi} = \sum_{n=A,B} \Omega_n^{\rm adi}(t)|P\rangle_n\langle e| + g_n|P\rangle_n\langle g| + \text{H.c.}, \tag{7}$$

describing a system with two neutral Λ-type atoms trapped in a cavity. The time-dependent Rabi frequencies are (see Fig. 3)

$$\begin{aligned}\Omega_A^{\rm adi} &= \frac{1}{\sqrt{2}}\Omega_0^{\rm adi}\exp\left[-(t - t_o - t_f/2)^2/t_c^2\right],\\ \Omega_B^{\rm adi} &= \frac{1}{\sqrt{2}}\Omega_0^{\rm adi}\exp\left[-(t - t_o - t_f/2)^2/t_c^2\right]\\ &\quad + \Omega_0^{\rm adi}\exp\left[-(t + t_o - t_f/2)^2/t_c^2\right].\end{aligned} \tag{8}$$

According to the result of comparison between Figs. 2(a) and 2(b), it is hard to say a dissipation-based scheme is better than a STIRAP one (even with a relatively small cooperativity C).

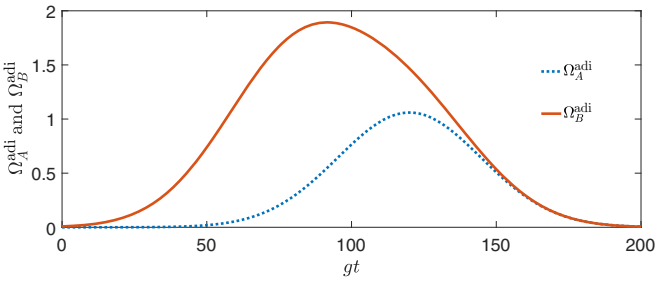

FIG. 3. Rabi frequencies in Eq. (8) of the STIRAP scheme. Parameters are chosen as $t_o = 20/g$, $t_c = 35/g$, and $\Omega_0^{\rm adi} = 0.15g$.

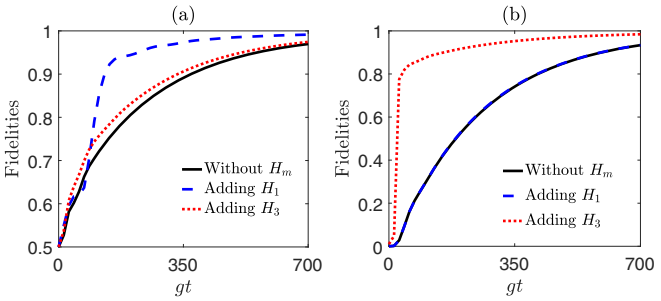

FIG. 4. The fidelities of singlet state $|S\rangle$ with and without adding ACC fields. (a) The initial state [see Eq. (14)] is chosen with $o = 1$ and intensity-dependent coefficients are $\mu_1 = 0.3g$ for the blue-dashed curve and $\mu_3 = 0.2g$ for the red-dotted curve. (b) The initial state [see Eq. (14)] is chosen with $o = 0.02$ and intensity-dependent coefficients are $\mu_1 = 0.3g$ and $\mu_3 = 0.2g$. Parameters are $\Omega = 0.07g$, $\omega = 0.02g$, $\Xi = 5g$, and $\Delta = 100g$. The decay rates are $\gamma = 0.1g$, $\kappa = 0$, and $\Gamma = 0.001g$.

When $C = 8.33$, the fidelity of a STIRAP scheme is about 89%, which is only a little lower than the fidelity of 90% of a dissipation-based scheme. However, the time required in a STIRAP scheme, i.e., $200/g$, is much shorter than that of about $700/g$ in a dissipation-based scheme. Therefore, to make sense of a dissipation-based scheme in practice, it is of significance to shorten the time required to stabilize a dissipative system.

We know that the fastest way to drive a quantum system to the target state is using coherent unitary dynamics. Therefore, to accelerate the slow dissipation process for entanglement generation, we add some ACC fields to the system. The ACC fields should be easily realized in practice. For the current system, the ACC Hamiltonians can be chosen as

$$\begin{aligned} H_1 &= \mu_1|e\rangle_A\langle p| + \text{H.c.}, \quad H_2 = \mu_2|e\rangle_B\langle p| + \text{H.c.}, \\ H_3 &= \mu_3|g\rangle_A\langle e| + \text{H.c.}, \quad H_4 = \mu_4|g\rangle_B\langle e| + \text{H.c.}, \end{aligned} \tag{9}$$

where μ_m ($m = 1,2,3,4$) are usually time-independent coefficients used to control the intensities of the ACC fields. The dynamics of the effective system after adding the ACC fields is governed by

$$\begin{aligned} \dot{\rho} &= -i[H_{\rm eff} + H_a, \rho] + \mathcal{L}\rho, \\ \mathcal{L}\rho &= \sum_k L_k^e \rho \left(L_k^e\right)^\dagger - \frac{1}{2}\left[\left(L_k^e\right)^\dagger L_k^e \rho + \rho\left(L_k^e\right)^\dagger L_k^e\right], \end{aligned} \tag{10}$$

with $H_a = \sum_m f_m(t) H_m$. Here, the control functions $f_m(t)$ can be regarded as the Rabi frequencies for the ACC fields. In this case, the instantaneous speed of the system becomes

$$\begin{aligned} v_a &= \langle S|\dot{\rho}|S\rangle \\ &= \frac{\gamma}{4}\langle\phi_0|\rho|\phi_0\rangle - i\langle S|[H_a,\rho]|S\rangle \\ &= \frac{\gamma}{4}\langle\phi_0|\rho|\phi_0\rangle - i\sum_m [f_m(t)\langle S|[H_m,\rho]|S\rangle]. \end{aligned} \tag{11}$$

Obviously, in order to improve the evolution speed, the second term in the last line of Eq. (11) should be ensured positive. For this goal, according to Lyapunov control [59], the control functions can be chosen as

$$f_m(t) = -i\langle S|[H_m,\rho]|S\rangle, \tag{12}$$

which are target-state-dependent functions. Beware that $\langle S|[H_m,\rho]|S\rangle$ are purely imaginary numbers; there is a negative sign in Eq. (12). The control functions mainly dependent on the definition of fidelity for the target state, when the definition is changed, will be accordingly changed. For example, when the fidelity is defined as $F = \text{Tr}[\sqrt{\rho_s}\rho\sqrt{\rho_s}]$, the expression for control functions becomes

$$f_m(t) = \text{Tr}[\sqrt{\rho_s}(-i[H_m,\rho])\sqrt{\rho_s}], \tag{13}$$

where $\rho_s = |S\rangle\langle S|$.

The principle to accelerate the evolution by adding ACC fields can be in fact understood as follows. The Hamiltonian H_0 is just used to guarantee that $|S\rangle$ is a steady state according to Eqs. (4) and (5), while, by adding the ACC fields, it is easy to find $(H_0 + H_a)|S\rangle \neq 0$ (for $\rho \neq \rho_s$ corresponding to $t < t_f$), which means $|S\rangle$ is actually not a steady state when $t < t_f$. For $t \to t_f$, according to Eq. (12), we have $f_m(t_f) = 0$ since $\rho|_{t=t_f} \to \rho_s$. Thus, $H_a = 0$, so that $|S\rangle$ becomes the unique steady state when $t \to t_f$. That is, when $t < t_f$, the coherent fields and dissipation work together to drive the system to state $|S\rangle$, while when $t \to t_f$ the ACC fields vanish and the system becomes steady. It can also be understood as that, in the current scheme, $|S\rangle$ is not a steady state until the population of the whole system is totally transferred to it.

By adding a suitable ACC field, such as $H_a = f_1(t)H_1 = f_1(t)\mu_1|e\rangle_A\langle p| + \text{H.c.}$, the fidelity versus time of the speed-up scheme is plotted in Fig. 4(c). Shown in the figure, in the speed-up scheme, the time required to stabilize the system seems independent to the decay rates. For an arbitrary cooperativity C, an evolution time $700/g$ seems enough to stabilize the system when a suitable ACC field is applied. To show this in more detail, we plot F versus C in Fig. 2(d). We can find, for a relatively large cooperativity, i.e., $C = 500$, for the scheme in Ref. [51], an evolution time $t_f = 5000/g$ is still not enough to stabilize the system, but an evolution time $t_f = 700/g$ is enough for the current speed-up scheme. Taking a comparison between Figs. 2(b) and 2(c), the time required in the current speed-up scheme is only about three times longer than that in a STIRAP scheme, while the fidelity of the speed-up scheme can be higher than that of a STIRAP scheme. Therefore, the current speed-up scheme can be an alternative choice in practice.

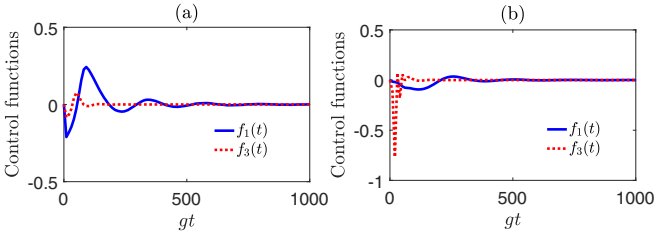

FIG. 5. The control functions given according to Eq. (12) for the accelerated dynamics with different initial states. The blue solid curves correspond to the situation that only ACC Hamiltonian H_1 is added and the red dotted curves correspond to the situation that only H_3 is added. (a) The initial state is chosen with $o = 1$ and the intensity-dependent coefficients are $\mu_1 = 0.3g$ for the blue-solid curve and $\mu_3 = 0.2g$ for the red-dotted curve. (b) The initial state is chosen with $o = 0.02$ and the intensity-dependent coefficients are $\mu_1 = 0.3g$ for the blue-solid curve and $\mu_3 = 0.2g$ for the blue-solid curve. Parameters are $\Omega = 0.07g$, $\omega = 0.02g$, $\Xi = 5g$, and $\Delta = 100g$. The decay rates are $\gamma = 0.1g$, $\kappa = 0$, and $\Gamma = 0.001g$.

IV. ANALYSIS AND DISCUSSION ON THE ACCELERATED STEADY-STATE ENTANGLEMENT GENERATION

First of all, we would like to study how the four ACC Hamiltonians behave in accelerating the entanglement generation. To ensure that the conditions for obtaining the effective Hamiltonian in Eq. (4) are satisfied, we choose parameters $\Omega = 0.07g$, $\omega = 0.02g$, $\Xi = 5g$, and $\Delta = 100g$. In the following analysis, the initial state for the system is assumed as

$$\rho_0 = [o|eg\rangle\langle eg| + (1-o)|gg\rangle\langle gg|] \otimes |0\rangle_c\langle 0|, \qquad (14)$$

where o is an undetermined coefficient. We independently display the fidelity of the singlet state $|S\rangle$ versus time in Fig. 4(a) when the ACC Hamiltonians H_1 (see the blue dashed curve) and H_3 (see the red dotted curve) are added. The effect of H_2 (H_4) on evolution is similar to H_1 (H_3) and does not deserve a separate discussion. The initial state is chosen as $\rho_0 = |eg\rangle\langle eg| \otimes |0\rangle_c\langle 0|$ in Fig. 4(a). Shown in the figure, by adding the ACC Hamiltonian H_1, the entanglement generation is significantly accelerated ($gt = 250$ is enough for a fidelity $\geqslant 95\%$), while, by adding H_3, the evolution is almost unchanged. That is, when the initial state is chosen with $o = 1$, the ACC Hamiltonian H_3 (H_4) is unable to accelerate the evolution. When we change the initial state to $\rho_0 = 0.02|eg\rangle\langle eg| \otimes |0\rangle_c\langle 0| + 0.98|eg\rangle\langle eg| \otimes |0\rangle_c\langle 0|$ (the following discussion shows that $o = 0.02$ is the best choice in this case), the result becomes different [see Fig. 4(b)] in that H_3 (H_4) can accelerate the evolution while H_1 (H_2) cannot. This result can be understood by Fig. 5, where the corresponding control functions are plotted. Figures 5(a) and 5(b) are plotted with initial conditions $o = 1$ and 0.02, respectively. In Fig. 5, the blue solid curves represent the control function $f_1(t)$ versus time under different conditions, and the red dotted curves represent $f_3(t)$ versus time. As we can find, the red dotted curve in Fig. 5(a) and the blue solid curve in Fig. 5(b) are close to the zero line, which means the corresponding ACC fields are too weak to accelerate the dynamics. The blue solid curve in Fig. 5(a) and the red dotted curve in Fig. 5(b) vanish gradually in an oscillating way along with the increasing of time. This verifies the ACC fields vanish after a certain evolution time

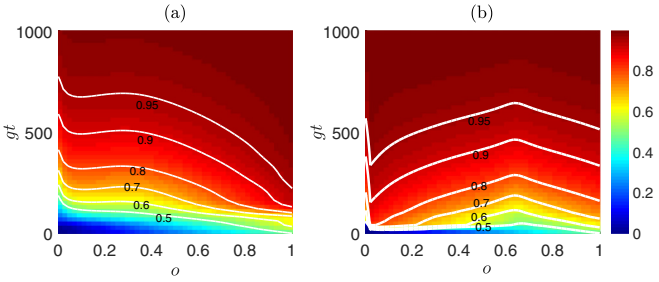

FIG. 6. The fidelity of singlet state $|S\rangle$ is plotted as a function of o, where o is given according to the initial state $\rho_0 = [o|eg\rangle\langle eg| + (1-o)|gg\rangle\langle gg|] \otimes |0\rangle_c\langle 0|$ ($o \in [0,1]$). (a) The ACC field is $f_1(t)H_1$ with $\mu_1 = 0.3g$. (b) The ACC field is $f_3(t)H_3$ with $\mu_3 = 0.2g$. Parameters are $\Omega = 0.07g$, $\omega = 0.02g$, $\Xi = 5g$, and $\Delta = 100g$. The decay rates are $\gamma = 0.1g$, $\kappa = 0$, and $\Gamma = 0.001g$.

so that the final stability of the system is guaranteed. The comparison between Figs. 5(a) and 5(b) shows us that H_1 is a better choice than H_3 to be chosen for the accelerated dynamics because the shape of $f_1(t)$ in Fig. 5(a) is easier to realize than that of $f_3(t)$ in Fig. 5(b). Moreover, it can be found from Fig. 4 that the choice of ACC Hamiltonian depends on the initial state. This point also can be demonstrated by Fig. 6, that shows the relationship between the fidelity and the initial state. According to Fig. 6, for the ACC Hamiltonian H_1, the evolution is accelerated more remarkably when o is closer to 1, while for H_3 the best choice is $o \to 0.02$. Additionally, the comparison between Figs. 4(a) and 4(b) [or Figs. 6(a) and 6(b)] also demonstrates that the ACC Hamiltonian H_1 (H_2) behaves better than H_3 (H_4) in accelerating the evolution.

The combined effect of ACC Hamiltonians H_1 and H_2 on the accelerated dynamics [see Fig. 7(a)] shows the acceleration effect cannot be improved by simply adding more same-type ACC fields or increasing the pulse intensity. The combined effect of different-type ACC Hamiltonians, i.e., H_1 and H_3, is given in Fig. 7(b). As compared to Fig. 7(a), adding different-type ACC Hamiltonians simultaneously has the ability to slightly improve the fidelity, i.e., $F \simeq 99\%$ when $\mu_1 \approx 0.3g$ and $\mu_3 \approx 0.1g$. That is, a high-fidelity steady-state entanglement generation is achievable by suitably choosing ACC fields with suitable intensities. However, the operation complexity may increase when adding more ACC fields. So,

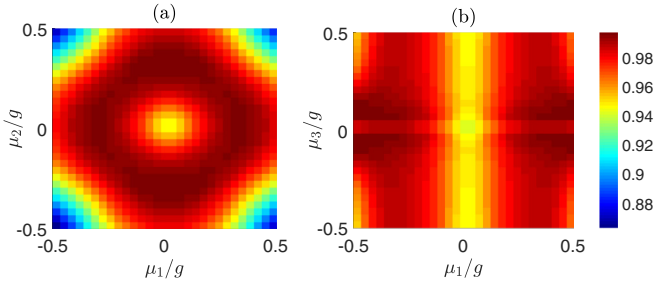

FIG. 7. The combined effect of different ACC Hamiltonians on the accelerated dynamics. (a) The fidelity of state $|S\rangle$ at the time $t = 500/g$ vs ACC fields' intensities μ_1 and μ_2. (b) The fidelity of state $|S\rangle$ at the time $t = 500/g$ vs ACC fields' intensities μ_1 and μ_3. Parameters are $\Omega = 0.07g$, $\omega = 0.02g$, $\Xi = 5g$, and $\Delta = 100g$. The decay rates are $\gamma = 0.1g$, $\kappa = 0$, and $\Gamma = 0.001g$.

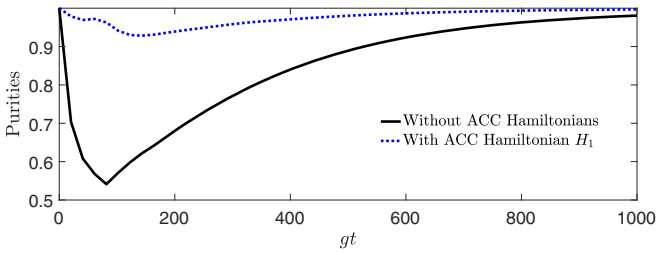

FIG. 8. The purity $P(t) = \mathrm{Tr}[\rho^2]$ is plotted as a function of time with initial state $|eg\rangle \otimes |0\rangle_c$. The black solid and blue dashed curves denote the purities for the general dissipation dynamics and the current accelerated dynamics, respectively. The initial state is $|eg\rangle \otimes |0\rangle_c$ and parameters are $\Omega = 0.07g$, $\omega = 0.02g$, $\Xi = 5g$, $\Delta = 100g$, and $\mu_1 = 0.3g$. The decay rates are $\gamma = 0.1g$, $\kappa = 0$, and $\Gamma = 0.001g$.

for convenience, in the following, we focus on analyzing the accelerated entanglement generation by adding the single ACC Hamiltonian H_1.

We define the purity of a quantum system as $P(t) = \mathrm{Tr}[\rho^2]$. The time evolutions of purities for the system with and without the ACC Hamiltonian H_1 are plotted in Fig. 8. We can find from the figure that the ACC Hamiltonian H_1 in fact protects the system from dissipation for a certain period of time, so that the starting point for convergence process is higher than that in a system without ACC Hamiltonians [the lowest purities in Figs. 8(a) and 8(b) are about 0.96 and 0.55, respectively]. Hence, the convergence time is shortened. In Figs. 9(a) and 9(b), we display the fidelities of state $|S\rangle$ versus Ω and ω, respectively. The result shows the ACC Hamiltonian H_1 behaves the best in accelerating the entanglement generation when the Zeno requirement is just satisfied: $\Omega \sim 0.1g$ and $\omega \sim 0.05g$. Although the Zeno requirement is fulfilled better with smaller Ω and ω, the evolution time is unacceptable long. The reason can be understood by the fact that when the Rabi frequency Ω is too small the system is slowly excited to the effective excited state $|\phi_0\rangle$. As shown in the effective transitions of the system [see Fig. 1(b)], a certain population for the effective excited state $|\phi_0\rangle$ is necessary for the convergence process, and the convergence time will be long if it is too slow to excite the system to $|\phi_0\rangle$.

For the current available parameters in the cavity QED with Rydberg-blocked atoms [76–78], the strength coupling

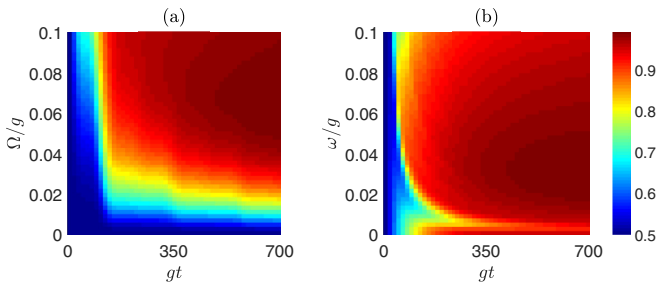

FIG. 9. The choice of optimal parameters Ω and ω for the accelerated dynamics. (a) The fidelity vs Ω and gt. (b) The fidelity vs ω and gt. The initial state is $|eg\rangle \otimes |0\rangle_c$ and parameters are $\Xi = 5g$, $\Delta = 100g$, and $\mu_1 = 0.3g$. The decay rates are $\gamma = 0.1g$, $\kappa = 0$, and $\Gamma = 0.001g$.

the transition between atomic ground level $5S_{1/2}$ and the optical level $5P_{3/2}$ of the ^{87}Rb atom to the quantized cavity mode is $g/2\pi = 55$ MHz, the decay rate of the intermediate state $|p\rangle$ is $\gamma/2\pi = 3$ MHz, the decay rate of the cavity mode is $\kappa/2\pi = 1$ MHz, and the spontaneous emission rate for the Rydberg state $95d_{5/2}$ of the ^{87}Rb atom is 0.03 MHz. By modulating the Rabi frequencies, detuning parameter, and Rydberg interaction strength satisfying $\Omega = 0.07g$, $\omega = 0.02g$, and $\lambda = 0.5g$, the time required to generate a high-fidelity ($\geqslant 98\%$) steady-state entanglement is only about 1.5 μs ($t_f \sim 500/g$ and $g = 55 \times 2\pi$ MHz).

V. ROBUSTNESS AGAINST STOCHASTIC PARAMETER FLUCTUATIONS

Figure 9 in fact indirectly demonstrates that the current accelerated scheme is robust against the systematic errors. The systematic errors are caused by fixed fluctuations on the parameters. For example, the fluctuation of Rabi frequency Ω can be assumed as a fixed value $\delta\Omega = \Omega' - \Omega$ with Ω' being the real value in experiment. As shown in Fig. 9, when $\Omega \sim 0.07g$ and $\omega \sim 0.02g$, the fidelity keeps almost unchanged with the slight changes of Ω and ω. That is, the system is robust against systematic errors. Therefore, in this section, we focus on analyzing the influence of a stochastic kind of noise on the fidelity. Assume that the Hamiltonian H_0 is perturbed by some stochastic part ηH_s describing amplitude noise. A stochastic Schrödinger equation in a close system (in the Stratonovich sense) is then $\dot{\psi}(t) = [H_0 + \eta H_s \xi(t)]\psi(t)$, where $\xi(t) = \partial_t W_t$ is heuristically the time derivative of the Brownian motion W_t. $\xi(t)$ satisfies $\langle \xi(t) \rangle = 0$ and $\langle \xi(t)\xi(t') \rangle = \delta(t - t')$ because the noise should have zero mean and the noise at different times should be uncorrelated. Then, we define $\rho_\xi(t) = |\psi_\xi(t)\rangle\langle\psi_\xi(t)|$, and the dynamical equation without dissipation terms for ρ_ξ is thus given as

$$\dot{\rho}_\xi = -i[H_0, \rho_\xi] - i\eta[H_s, \xi\rho_\xi]. \tag{15}$$

After averaging over the noise, Eq. (15) becomes

$$\dot{\rho} \simeq -i[H_0, \rho] - i\eta[H_s, \langle \xi\rho_\xi \rangle], \tag{16}$$

where $\rho = \langle \rho_\xi \rangle$ [79]. According to Novikov's theorem in case of white noise, we have $\langle \xi\rho_\xi \rangle = \frac{1}{2}\langle \frac{\delta\rho_\xi}{\delta\xi(t')} \rangle|_{t'=t} = -\frac{i\eta}{2}[H_s, \rho]$. Thus, when both the noise and the dissipation are taken into account, the system evolution is governed by

$$\dot{\rho} = -i[H_0, \rho] + \mathcal{L}\rho + \mathcal{N}\rho, \tag{17}$$

where $\mathcal{N}\rho = -\eta^2[H_s, [H_s, \rho]]/2$. Adding the ACC Hamiltonians, Eq. (17) becomes

$$\dot{\rho} = -i[H_0 + H_a, \rho] + \mathcal{L}\rho + \mathcal{N}\rho. \tag{18}$$

We choose $H_a = f_1(t)H_1$ in the following analysis. Beware that the control function $f_1(t)$ is given according to the master equation in Eq. (10) without the noise terms.

For the current scheme, we consider the amplitude noises exist in

$$\begin{aligned} H_{s1} &= \Omega|p\rangle_A\langle e| + \mathrm{H.c.}, \\ H_{s2} &= \omega|g\rangle_A\langle e| + \mathrm{H.c.}, \\ H_{s3} &= U_{rr}|rr\rangle\langle rr|, \end{aligned} \tag{19}$$

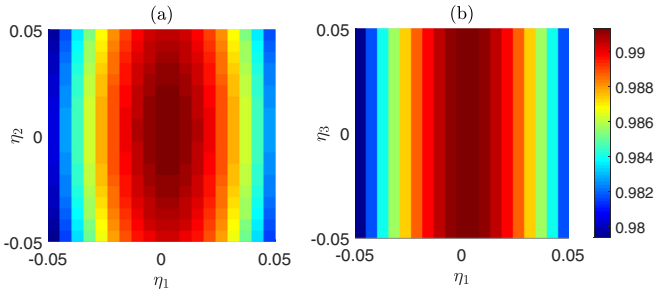

FIG. 10. The robustness of the accelerated dynamics against stochastic parameter fluctuations when $t_f = 700/g$. (a) The fidelity vs η_1 and η_2 denoting the amplitude noise intensities of Ω and ω, respectively. (b) The fidelity vs η_1 and η_3 denoting the amplitude noise intensities of Ω and U_{rr}, respectively. The initial state is $|eg\rangle \otimes |0\rangle_c$ and parameters are $\Omega = 0.07g$, $\omega = 0.02g$, $\Xi = 5g$, $\Delta = 100g$, and $\mu_1 = 0.3g$. The decay rates are $\gamma = 0.1g$, $\kappa = 0$, and $\Gamma = 0.001g$.

with intensities η_1^2, η_2^2, and η_3^2, respectively. The last line in Eq. (19) is considered because it is difficult to accurately adjust the distance between two Rydberg atoms in experiment. In Fig. 10, we simulate the steady-state fidelity as a function of $\eta_{1,(2,3)}$ to analyze the influence of amplitude noises. Fortunately, the current scheme is robust against the amplitude noises caused by the microwave field and the Rydberg-mediated interaction, and the scheme permits $\eta_{2,(3)} \in [-5\%, 5\%]$ so as to preserve the fidelity almost unchanged. For error Hamiltonian H_{s1}, the negative effect of amplitude noise on the fidelity is also very small: only 1% deviation is caused even when the noise intensities are $\eta_1 = \eta_2 = \eta_3 = 0.05$. That is, the accelerated scheme is demonstrated to be robust against amplitude-noise errors.

VI. CONCLUSION

In conclusion, we have proposed a scheme based on Lyapunov control to accelerate the generation of steady-state entanglement in a cavity QED system with Rydberg atoms. The ACC fields in fact protect the system from dissipation in a certain time. Thus an imperfect unitary evolution is allowed for the system to rapidly reach the target steady state with fidelity about 90% in the first evolution stage. Then, in the second evolution stage, the ACC fields gradually vanish and the dissipation dynamics occupies a leading position to converge the system to target steady state (from fidelity ~90 to ~100%). Numerical simulation demonstrates that the time required for entanglement generation with fidelity $\geqslant 95\%$ has been shortened by about six times as compared to that for a scheme without ACC fields. Moreover, the accelerated scheme is robust against noise errors as demonstrated by numerical simulation. As a result, the current scheme combining the advantages of coherent unitary dynamics and dissipation dynamics allows for significant improvement in quantum entanglement generation. Therefore, we hope that the current paper may open venues for the experimental realization of entanglement in the near future.

ACKNOWLEDGMENTS

This paper was supported by the National Natural Science Foundation of China under Grants No. 11575045, No. 11374054, and No. 11675046.

APPENDIX: QUANTUM ZENO DYNAMICS

The quantum Zeno effect, which has been tested in many experiments, is the inhibition of transitions between quantum states by frequent measurements [80–83]. It shows that a system can actually evolve away from its initial state while it still remains in the so-called Zeno subspace determined by the measurement when frequently projected onto a multidimensional subspace. This was called "quantum Zeno dynamics" (QZD) by Facchi and Pascazio in 2002 [67]. In fact, QZD can be achieved via continuous coupling between the system and an external system instead of discontinuous measurements. Here, we give an elementary introduction to this kind of QZD. A generic Hamiltonian of a dynamical evolution can be written as

$$H = H_c + K H_p, \tag{A1}$$

where H_c is the Hamiltonian of the quantum system, H_p is an interaction Hamiltonian caricaturing the continuous measurement, and K is the coupling constant. In the strong-coupling limit, $K \to \infty$, the subsystem of interest is dominated by the evolution operator

$$\begin{aligned} U_0(t) &= \lim_{K\to\infty} \exp(iKH_p t)U(t) \\ &= \exp\left(-it\sum_n P_n H_c P_n\right), \end{aligned} \tag{A2}$$

where P_n is the projector onto the space of eigenstates of H_p with eigenvalues ζ_n, i.e., $H_p = \sum_n \zeta_n P_n$. Thus, the whole system is governed by the limiting evolution operator

$$\begin{aligned} U(t) &= \exp(-iKH_p t)U_0(t) \\ &= \exp\left[-it\sum_n (K\zeta_n P_n + P_n H_c P_n)\right]. \end{aligned} \tag{A3}$$

The effective Hamiltonian (also known as the "Zeno Hamiltonian") for the system is accordingly given as

$$H_Z = \sum_n (K\zeta_n P_n + P_n H_c P_n). \tag{A4}$$

In the current scheme, we consider H_{ac} as KH_p and H_r as H_c, and the strong-coupling limit $K \to \infty$ corresponds to $g \gg \Omega$. According to Eq. (A4) and Ref. [51], the effective Hamiltonian in Eq. (4) can be obtained.

[1] E. Torrontegui, S. Ibáñez, S. Martínez-Garaot, M. Modugno, A. del Campo, D. Gué-Odelin, A. Ruschhaupt, X. Chen, and J. G. Muga, Adv. Atom. Mol. Opt. Phys. **62**, 117 (2013).

[2] X. Chen, I. Lizuain, A. Ruschhaupt, D. Guéry-Odelin, and J. G. Muga, Phys. Rev. Lett. **105**, 123003 (2010).

[3] A. del Campo, Phys. Rev. Lett. **111**, 100502 (2013).

[4] S. Ibáñez, X. Chen, E. Torrontegui, J. G. Muga, and A. Ruschhaupt, Phys. Rev. Lett. **109**, 100403 (2012).

[5] A. Baksic, H. Ribeiro, and A. A. Clerk, Phys. Rev. Lett. **116**, 230503 (2016).

[6] Y. H. Chen, Y. Xia, Q. C. Wu, B. H. Huang, and J. Song, Phys. Rev. A **93**, 052109 (2016); Y. H. Chen, Z. C. Shi, J. Song, Y. Xia, and S. B. Zheng, *ibid.* **95**, 062319 (2017).

[7] A. del Campo, Phys. Rev. A **84**, 031606(R) (2011); Eur. Phys. Lett. **96**, 60005 (2011).

[8] S. An, D. Lv, A. del Campo, and K. Kim, Nat. Commun. **7**, 12999 (2016).

[9] X. Chen and J. G. Muga, Phys. Rev. A **86**, 033405 (2012).

[10] S. Ibáñez, S. Martínez-Garaot, X. Chen, E. Torrontegui, and J. G. Muga, Phys. Rev. A **84**, 023415 (2011).

[11] X. Chen, E. Torrontegui, and J. G. Muga, Phys. Rev. A **83**, 062116 (2011).

[12] S. Ibáñez and J. G. Muga, Phys. Rev. A **89**, 033403 (2014).

[13] S. Ibáñez, X. Chen, and J. G. Muga, Phys. Rev. A **87**, 043402 (2013).

[14] A. C. Santos, R. D. Silva, and M. S. Sarandy, Phys. Rev. A **93**, 012311 (2016).

[15] T. Opatrný and K. Mølmer, New J. Phys. **16**, 015025 (2014).

[16] H. Saberi, T. Opatrny, K. Mølmer, and A. del Campo, Phys. Rev. A **90**, 060301(R) (2014).

[17] Y. H. Chen, Y. Xia, Q. Q. Chen, and J. Song, Phys. Rev. A **89**, 033856 (2014).

[18] Y. X. Du, Z. T. Liang, Y. C. Li, X. X. Yue, Q. X. Lv, W. Huang, X. Chen, H. Yan, and S. L. Zhu, Nat. Commun. **7**, 12479 (2016).

[19] B. B. Zhou, A. Baksic, H. Ribeiro, C. G. Yale, F. J. Heremans, P. C. Jerger, A. Auer, G. Burkard, A. A. Clerk, and D. D. Awschalom, Nat. Phys. **13**, 330 (2017).

[20] Y. H. Kang, Y. H. Chen, Z. C. Shi, J. Song, and Y. Xia, Phys. Rev. A **94**, 052311 (2016).

[21] B. H. Huang, Y. H. Kang, Y. H. Chen, Q. C. Wu, J. Song, and Y. Xia, Phys. Rev. A **96**, 022314 (2017).

[22] M. Lu, Y. Xia, L. T. Shen, J. Song, and N. B. An, Phys. Rev. A **89**, 012326 (2014).

[23] Y. H. Chen, Y. Xia, Q. Q. Chen, and J. Song, Phys. Rev. A **91**, 012325 (2015).

[24] B. T. Torosov, G. Della Valle, and S. Longhi, Phys. Rev. A **87**, 052502 (2013); **89**, 063412 (2014).

[25] G. Vacanti, R. Fazio, S. Montangero, G. M. Palma, M. Paternostro, and V. Vedral, New J. Phys. **16**, 053017 (2014).

[26] A. Sala, D. L. Núñez, J. Martorell, L. DeSarlo, T. Zibold, F. Gerbier, A. Polls, and B. Juliá-Díaz, Phys. Rev. A **94**, 043623 (2016).

[27] S. Deffner, New J. Phys. **18**, 012001 (2016).

[28] X. K. Song, F. G. Deng, L. Lamata, and J. G. Muga, Phys. Rev. A **95**, 022332 (2017).

[29] S. Campbell and S. Deffner, Phys. Rev. Lett. **118**, 100601 (2017).

[30] K. Funo, J. N. Zhang, C. Chatou, K. Kim, M. Ueda, and A. del Campo, Phys. Rev. Lett. **118**, 100602 (2017).

[31] M. J. Kastoryano, F. Reiter, and A. S. Sørensen, Phys. Rev. Lett. **106**, 090502 (2011).

[32] X. T. Wang and S. G. Schirmer, arXiv:1005.2114v2 (2010).

[33] G. Vacanti and A. Beige, New J. Phys. **11**, 083008 (2009).

[34] R. Blatt and D. Wineland, Nature (London) **453**, 1008 (2008).

[35] B. Baumgartner, H. Narnhofer, and W. Thirring, J. Phys. A **41**, 065201 (2008).

[36] F. Verstraete, M. M. Wolf, and J. I. Cirac, Nat. Phys. **5**, 633 (2009).

[37] Karl Gerd H. Vollbrecht, C. A. Muschik, and J. I. Cirac, Phys. Rev. Lett. **107**, 120502 (2011).

[38] E. G. Dalla Torre, J. Otterbach, E. Demler, V. Vuletic, and M. D. Lukin, Phys. Rev. Lett. **110**, 120402 (2013).

[39] F. Reiter, M. J. Kastoryano, and A. S. Sørensen, New J. Phys. **14**, 053022 (2012).

[40] D. Braun, Phys. Rev. Lett. **89**, 277901 (2002).

[41] L. Memarzadeh and S. Mancini, Phys. Rev. A **83**, 042329 (2011).

[42] A. F. Alharbi and Z. Ficek, Phys. Rev. A **82**, 054103 (2010).

[43] J. Busch, S. De, S. S. Ivanov, B. T. Torosov, T. P. Spiller, and A. Beige, Phys. Rev. A **84**, 022316 (2011).

[44] X. L. Wang, L. K. Chen, W. Li, H. L. Huang, C. Liu, C. Chen, Y. H. Luo, Z. E. Su, D. Wu, Z. D. Li, H. Lu, Y. Hu, X. Jiang, C. Z. Peng, L. Li, N. L. Liu, Y. A. Chen, C. Y. Lu, and J. W. Pan, Phys. Rev. Lett. **117**, 210502 (2016).

[45] L. T. Shen, X. Y. Chen, Z. B. Yang, H. Z. Wu, and S. B. Zheng, Phys. Rev. A **84**, 064302 (2011).

[46] H. Krauter, C. A. Muschik, K. Jensen, W. Wasilewski, J. M. Petersen, J. I. Cirac, and E. S. Polzik, Phys. Rev. Lett. **107**, 080503 (2011).

[47] Y. Lin, J. P. Gaebler, F. Reiter, T. R. Tan, R. Bowler, A. S. Sørensen, D. Leibfried, and D. J. Wineland, Nature (London) **504**, 415 (2013).

[48] S. Shankar, M. Hatridge, Z. Leghtas, K. M. Sliwa, A. Narla, U. Vool, S. M. Girvin, L. Frunzio, M. Mirrahimi, and M. H. Devoret, Nature (London) **504**, 419 (2013).

[49] A. W. Carr and M. Saffman, Phys. Rev. Lett. **111**, 033607 (2013).

[50] D. D. Bhaktavatsala Rao and K. Mølmer, Phys. Rev. Lett. **111**, 033606 (2013).

[51] X. Q. Shao, J. H. Wu, and X. X. Yi, Phys. Rev. A **95**, 022317 (2017).

[52] X. Q. Shao, J. H. Wu, and X. X. Yi, Phys. Rev. A **95**, 062339 (2017).

[53] X. Q. Shao, D. X. Li, Y. Q. Ji, J. H. Wu, and X. X. Yi, Phys. Rev. A **96**, 012328 (2017).

[54] A. Neuzner, M. Körber, O. Morin, S. Ritter, and G. Rempe, Nat. Photonics **10**, 303 (2016).

[55] F. Reiter, D. Reeb, and A. S. Sørensen, Phys. Rev. Lett. **117**, 040501 (2016).

[56] G. Morigi, J. Eschner, C. Cormick, Y. Lin, D. Leibfried, and D. J. Wineland, Phys. Rev. Lett. **115**, 200502 (2015).

[57] F. Reiter and A. S. Sørensen, Phys. Rev. A **85**, 032111 (2012).

[58] D. d'Alessandro, *Introduction to Quantum Control and Dynamics* (CRC, Boca Raton, FL, 2007).

[59] S. Kuang and S. Cong, Automatica **44**, 98 (2008); Acta Automat. Sinica **36**, 1257 (2010).

[60] W. Cui and F. Nori, Phys. Rev. A **88**, 063823 (2013).

[61] Z. C. Shi, X. L. Zhao, and X. X. Yi, Phys. Rev. A **91**, 032301 (2015).

[62] J. M. Coron, A. Grigoriu, C. Lefter, and G. Turinici, New J. Phys. **11**, 105034 (2009).

[63] X. X. Yi, X. L. Huang, C. F. Wu, and C. H. Oh, Phys. Rev. A **80**, 052316 (2009).

[64] X. T. Wang and S. G. Schirmer, Phys. Rev. A **80**, 042305 (2009).

[65] J. Wen and S. Cong, Open Syst. Inf. Dyn. **23**, 1650005 (2016).

[66] W. Wang, L. C. Wang, and X. X. Yi, Phys. Rev. A **82**, 034308 (2010).

[67] P. Facchi and S. Pascazio, Phys. Rev. Lett. **89**, 080401 (2002); J. Phys. A **41**, 493001 (2008).
[68] D. Jaksch, J. I. Cirac, P. Zoller, S. L. Rolston, R. Côté, and M. D. Lukin, Phys. Rev. Lett. **85**, 2208 (2000).
[69] D. Møller, L. B. Madsen, and K. Mølmer, Phys. Rev. Lett. **100**, 170504 (2008).
[70] E. Urban, T. A. Johnson, T. Henage, L. Isenhower, D. D. Yavuz, T. G. Walker, and M. Saffman, Nat. Phys. **5**, 110 (2009).
[71] M. Saffman, T. G. Walker, and K. Mølmer, Rev. Mod. Phys. **82**, 2313 (2010).
[72] M. Müller, I. Lesanovsky, H. Weimer, H. P. Büchler, and P. Zoller, Phys. Rev. Lett. **102**, 170502 (2009).
[73] L. Isenhower, E. Urban, X. L. Zhang, A. T. Gill, T. Henage, T. A. Johnson, T. G. Walker, and M. Saffman, Phys. Rev. Lett. **104**, 010503 (2010).
[74] D. F. V. James and J. Jerke, Can. J. Phys. **85**, 625 (2007).
[75] G. Lindblad, Commun. Math. Phys. **48**, 119 (1976).
[76] F. Brennecke, T. Donner, S. Ritter, T. Bourdel, M. Köhl, and T. Esslinger, Nature (London) **450**, 268 (2007).
[77] A. Grankin, E. Brion, E. Bimbard, R. Boddeda, I. Usmani, A. Ourjoumtsev, and P. Grangier, New J. Phys. **16**, 043020 (2014).
[78] X. F. Zhang, Q. Sun, Y. C. Wen, W. M. Liu, S. Eggert, and A. C. Ji, Phys. Rev. Lett. **110**, 090402 (2013).
[79] A. Ruschhaupt, X. Chen, D. Alonso, and J. G. Muga, New J. Phys. **14**, 093404 (2014).
[80] B. Misra and E. C. G. Sudarshan, J. Math. Phys. **18**, 756 (1977).
[81] Wayne M. Itano, D. J. Heinzen, J. J. Bollinger, and D. J. Wineland, Phys. Rev. A **41**, 2295 (1990).
[82] P. Kwiat, H. Weinfurter, T. Herzog, A. Zeilinger, and M. A. Kasevich, Phys. Rev. Lett. **74**, 4763 (1995).
[83] R. J. Cook, Phys. Scr. T **21**, 49 (1988).